Computer-Aided Design of Slit-Coupled *H*-Plane T-Junction Diplexers with *E*-Plane Metal-Insert Filters

JOACHIM DITTLOFF AND FRITZ ARNDT, SENIOR MEMBER, IEEE

Abstract—A rigorous field theory design of a class of rectangular waveguide slit-coupled *H*-plane T-junction diplexers is described utilizing *E*-plane metal-insert filters. The filter elements allow low-cost manufacturing by accurate and inexpensive metal-etching techniques. The design method is based on field expansion in suitably normalized eigenmodes which yield the modal scattering matrix of three appropriate key building block structures to be combined, the *E*-plane metal-insert section, the *H*-plane iris discontinuity, and the *H*-plane T. The theory includes the finite thickness of the diaphragms as well as the higher order mode interaction of all discontinuities within the complete diplexer structure. Computer-optimized design data are given for diplexer examples in *Ku*-band (12–18 GHz) and *E*-band (60–90 GHz), designed for more than 23 dB common port return losses. The theory is verified by measured results for a five-resonator *Ku*-band diplexer.

I. Introduction

THE RECTANGULAR waveguide *H*-plane T-junction connected diplexer is an old and proved design [1]–[4] where commonly inductive iris or post coupled cavity channel filters [1] are used. Increasing progress in the construction of channelized receivers, especially at higher frequencies, however, has promted the need for compact and low-cost diplexers utilizing quasi-planar printed-circuit filter components [5]–[12]. Previous designs are based on quadrature hybrid [5]–[8], open *E*-plane tee [9], open *H*-plane tee [8], [10], and suspended probe coupling techniques [11], [12]. Additional coupling structures may cause additional loss and cost [5], [13]; open T-junction feeds are often difficult to match [2], [9], [10].

This paper describes the rigorous design of a class of slit-coupled *H*-plane T-junction diplexers (Fig. 1) with *E*-plane metal-insert filters in the main arm ("common junction type," Fig. 1(a)), in the side arms ("manifold type," Fig. 1(b)), and in the main and side arms ("modified common junction type," Fig. 1(c)). The slit-coupled *H*-plane T junction is a particularly useful circuit for this kind of diplexer since the same group of modes (TE_{m0}) is excited at the discontinuities as within the filter sections. Only three field components are required in the computations, which therefore reduces the computing time involved considerably. Moreover, the junction effects may be well compensated. *E*-plane integrated metal-insert filters achieve low insertion loss because of the absence of supporting dielectrics [9], [14]–[16].

Manuscript received April 7, 1988; revised June 28, 1988.

The authors are with the Microwave Depratment, University of Bremen, D-2800 Bremen 33, West Germany.

IEEE Long Number 8823771.

Previous design methods for diplexers using printed-circuit filters are based on empirical [5] or equivalent circuit techniques [6]–[8], [14], or on approximate methods for the feeding structures [10]–[12]. To ensure good overall performance, however, it may be desirable to include rigorously the loading effects of the filter structures as well as the higher order mode interactions between them and the feeding transitions. Moreover, rigorous design methods yield the advantage of utilizing the full mutual compensation potential inherent to the structure, and allow the stopband characteristics of the filters to be included in the diplexer design.

The computer-aided design method described, which is based on the field expansion into suitably normalized eigenmodes and the generalized modal scattering matrix formulation of interacting structures, has already been applied successfully in solving various waveguide scattering problems [15], [18], [19], [22]–[25]. This paper compiles those aspects of the theory which are relevant for designing the class of diplexers shown in Fig. 1. Although the modal *S* matrices of the individual *H*-plane step discontinuities are already available in [15], [18], and [19] and may be combined, therefore, by homogeneous waveguide sections between them [15], [18] or by superposition techniques [12], [25], respectively, it is numerically more adequate to use the appropriately composed key building block elements directly: the *E*-plane metal insert of finite length and thickness, the inductive iris of finite thickness, and the *H*-plane T.

The immediate modal *S*-matrix combination [15], [18] of the interacting key building block elements avoids numerical instabilities in the calculations. For computer optimization, the evolution strategy method [15], [18], [21] is utilized, where no differentiation step is necessary, and the problem of local minima may be circumvented. Design examples for optimized diplexers for *Ku*-band (12–18 GHz) and *E*-band (60–90 GHz) waveguides are given. The theory is experimentally verified by measured results of a *Ku*-band manifold-type diplexer.

II. Theory

Along the waveguide discontinuities of the slit-coupled *H*-plane junction connected diplexer structures (Fig. 1), only TE_{m0} modes are excited [20] for TE_{10} mode incidence at the feeding port. For the *H*-plane cross-sectional discon-

0018-9480/88/1200-1833$01.00

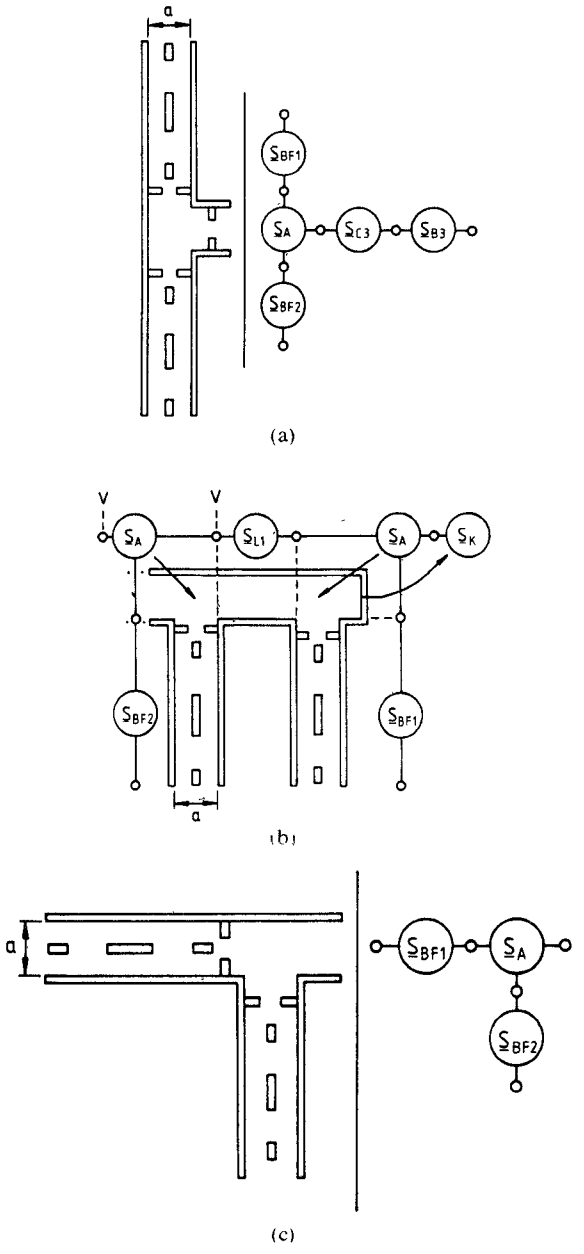

Fig. 1. Slit-coupled H-plane T-junction connected diplexers with E-plane metal-insert filters. Composed modal scattering matrices. (a) Filters in main arm (common junction type). (b) Filters in side arms (manifold type). (c) Filters in main and side arms (modified common junction type).

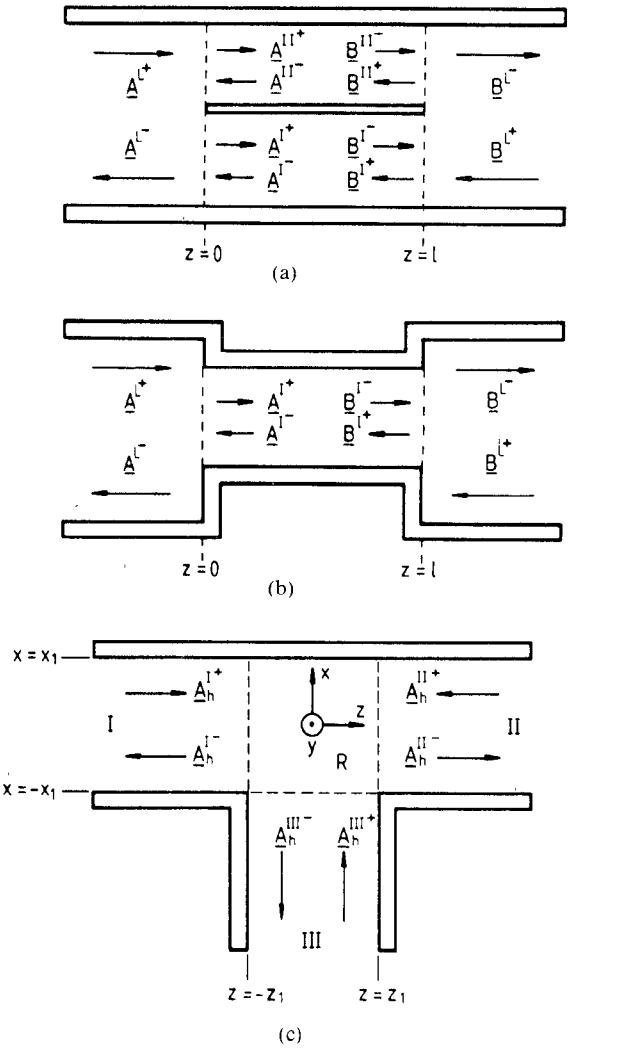

Fig. 2. Key building block structures for the calculation of the overall scattering matrix of the diplexers. (a) Metal strip coupling section of finite length. (b) Inductive iris coupling section of finite length. (c) H-plane T junction.

tinuities in Fig. 2(a) and (b), for the homogeneous waveguide subregion under consideration, the fields [20], [24]

$$\vec{E} = \nabla \times \left(\vec{Q}_{hz}\right)$$

$$\vec{H} = -\frac{1}{j\omega\mu}\nabla \times \nabla \times \left(\vec{Q}_{hz}\right) \tag{1a}$$

may be derived from the z component of the magnetic vector potential

$$Q_{hz}^{o} = \sum_{i^o}^{I^o} N_{hi^o}^{o} \cdot T_{hi^o}^{o} \cdot \left(A_{hi^o}^{o\pm} \cdot e^{\mp jk_{z_i o}^{o} z}\right) \tag{2a}$$

where $o = 1, 2, \cdots, M_s$ (M_s = total number of subregions at the corresponding discontinuity, e.g. $M_S = 3$ at $z = 0$ of Fig. 2(a)), and i^o is the index i for the I^o TE_0 modes considered in each subregion.

For the H-plane T junction (Fig. 2(c)), it has turned out to be adequate [19], [25] to utilize the field relations [20]

$$\vec{E} = \nabla \times \nabla \times \left(\Pi_{ey}\right)$$

$$\vec{H} = j\omega\epsilon\nabla \times \left(\Pi_{ey}\right) \tag{1b}$$

for the y component of the electrical Hertzian vector potential

$$\Pi_{ey}^{o} = \sum_{i^o}^{I^o} N_{ei^o}^{o} \cdot T_{ei^o}^{o} \cdot \left(A_{hi^o}^{o\pm} \cdot e^{\mp jk_{p_i o}^{o} p}\right). \tag{2b}$$

The symbols N and T in (2) denote, respectively, the normalization factor due to the complex power and the eigenfunctions in the corresponding subregions; $A^{\pm}$ are the amplitude coefficients of the forward and backward waves at the discontinuity under consideration (Fig. 2); k_z, k_q are the wavenumbers of the corresponding TE_{io} modes;

q and p in (2b) denote the corresponding cross section and propagation expressions, respectively, for the H-plane T (Fig. 2(c)). These kinds of discontinuities in Fig. 2 have already been explicitly treated in [15], [18], [19], and [25]; for further details, the reader is referred to the literature.

By matching the tangential field components at the common interfaces at the individual step discontinuities, the wave amplitude coefficients of (2) can be related to each other by taking the orthogonal properties of the modes into account [20]. This yields the modal scattering matrices [15], [18], [19] of the individual discontinuities (Fig. 2).

The composed *modal scattering matrices of the key building block filter coupling section elements*, metal strip (Fig. 2(a)) and inductive iris (Fig. 2(b)) of finite lengths, are usually calculated indirectly by combining the related matrices of the individual discontinuities: the scattering matrix at $z=0$, the scattering matrix of the homogeneous waveguide section(s) of finite length l, and the scattering matrix of the inverse structure at $z=l$ [15], [18]. However, in order to reduce the numerical requirements, it is more adequate to utilize the related modal S-matrix expressions directly, as given below:

$$\begin{pmatrix} (A^{L^-})_n \\ (B^{L^-})_n \end{pmatrix} = \begin{pmatrix} (S_{11})_n & (S_{12})_n \\ (S_{12})_n & (S_{11})_n \end{pmatrix} \begin{pmatrix} (A^{L^+})_n \\ (B^{L^+})_n \end{pmatrix} \tag{3}$$

where the index $n=1$ denotes the elements of the strip section (Fig. 2(a)) and $n=2$ those of the inductive iris section. The submatrices of the two key building block filter elements of Fig. 2(a) and (b) are elucidated in the Appendix ((A1)–(A10)).

The relations for the modal scattering matrix of the key building block *H-plane* T (Fig. 2(c)) are derived analogously to the E-plane T junction [22] by superimposing on the field in the cavity region R three suitably chosen standing wave solutions [19], [25]. The modal S matrix of the H-plane T is given by

$$\begin{pmatrix} (A_h^{\mathrm{I}^-}) \\ (A_h^{\mathrm{II}^-}) \\ (A_h^{\mathrm{III}^-}) \end{pmatrix} = \begin{pmatrix} (S_{11})_h & (S_{12})_h & (S_{13})_h \\ (S_{21})_h & (S_{22})_h & (S_{23})_h \\ (A_{31})_h & (S_{32})_h & (S_{33})_h \end{pmatrix} \begin{pmatrix} (A_h^{\mathrm{I}^+}) \\ (A_h^{\mathrm{II}^+}) \\ (A_h^{\mathrm{III}^+}) \end{pmatrix} \tag{4}$$

where the submatrices are also explicitly given in the Appendix ((A11)–(A29)).

For calculating the complete diplexer structures of Fig. 1, a direct combination of the modal scattering matrices of the key building block elements and of the intermediate homogeneous waveguide sections involved is used [15], [18], [23]. The general relations, which may be used iteratively to combine the two- and three-port modal scattering matrices of the diplexer structures (Fig. 1), are already formulated in [23]. The relations in [23] require only one matrix inversion per modal S matrix involved.

A computer program was written using the preceding relations and utilizing the evolution strategy method (cf. [15], [18], and [21]) for optimizing the geometrical parameters of the diplexers for given specifications. Sufficient asymptotic behavior has been obtained by consideration of 45 TE_{m0} modes at all discontinuities. This is demonstrated in Fig. 3 by plotting the behavior of parameters which are very sensitive to the number of modes included. Examples of this are the overall fundamental mode scattering parameters S_{21} ($\Delta\ \Delta\ \Delta$) of the diplexer example of Fig. 4, and S_{31} ($+\ +\ +$) of the diplexer example of Fig. 6(a) at a high frequency within the waveguide band under consideration at, for instance, $f=16$ GHz as a function of the number of TE_{m0} modes taken into account. The relatively high number of modes required indicates that the mutual higher order mode interaction at such complicated structures cannot be neglected if reliable computer-optimized design data are desired.

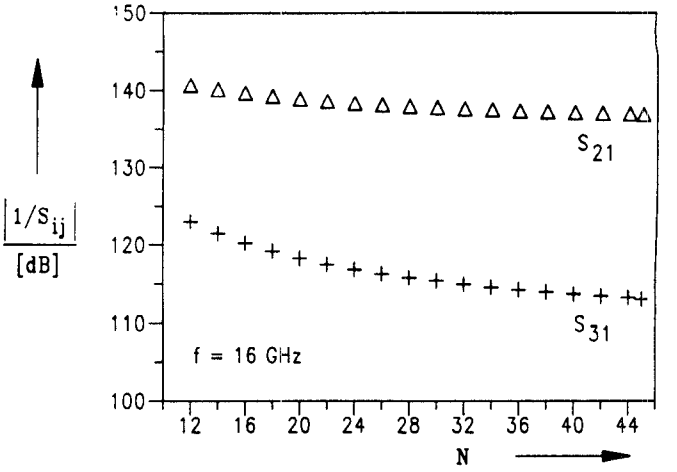

Fig. 3. Convergence behavior. Common port transmission coefficients S_{21} ($\Delta\ \Delta\ \Delta$) of the diplexer example of Fig. 4, and S_{31} ($+\ +\ +$) of the example of Fig. 6(a), at $f=16$ GHz, as a function of the number of TE_{m0} modes taken into account

III. Design and Results

The computer-aided design is advantageously carried out in two steps by an optimization program which applies the evolution strategy method, i.e., a suitably modified direct search procedure [15], [18], [21]. In the first step, the individual filters are optimized according to the given specifications. These results are utilized for the initial values in the second step, which comprises the total diplexer structure. The error function to be minimized in the first step is based on the calculation of the corresponding filter transmission coefficients, in both passband and stopband [15], [18]. For the overall diplexer optimization in the second step, the error function is based on the most critical design criterion, the return loss behavior of the common diplexer port within the frequency bands under consideration.

For given waveguide dimensions, metal insert and iris thicknesses, the parameter vector ($\bar{x}$) to be optimized includes: 1) the coupling section and resonator lengths for the E-plane metal insert filters, in the first optimization step; 2) the widths and location of the inductive irises in the junctions; 3) the distance between the irises and the

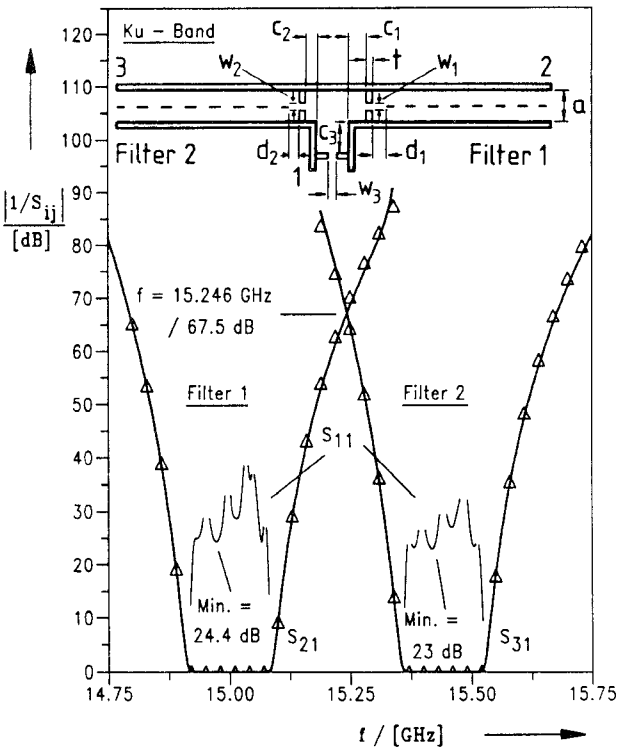

Fig. 4. Computer-optimized *Ku*-band common junction type diplexer with two seven-resonator *E*-plane metal-insert Filters. Common port scattering coefficients S_{21} and S_{31} compared with the corresponding single transmission coefficients of the individual filters (Δ Δ Δ). The filter dimensions are given in Table I.

$a = 15.799$ mm, $b = 7.899$ mm, $t = 1$ mm
filter 1: $f_0 = 15$ GHz, $B/f_0 = 0.012$
filter 2: $f_0 = 15.44$ GHz, $B/f_0 = 0.0117$
$w_1 = 13.219$ mm, $c_1 = 8.664$ mm, $d_1 = 0.3109$ mm
$w_2 = 12.886$ mm, $c_2 = 6.258$ mm, $d_2 = 0.8168$ mm
$w_3 = 12\,265$ mm, $c_3 = 3.142$ mm
(f_0 = midband frequency; B/f_0 = relative bandwidth).

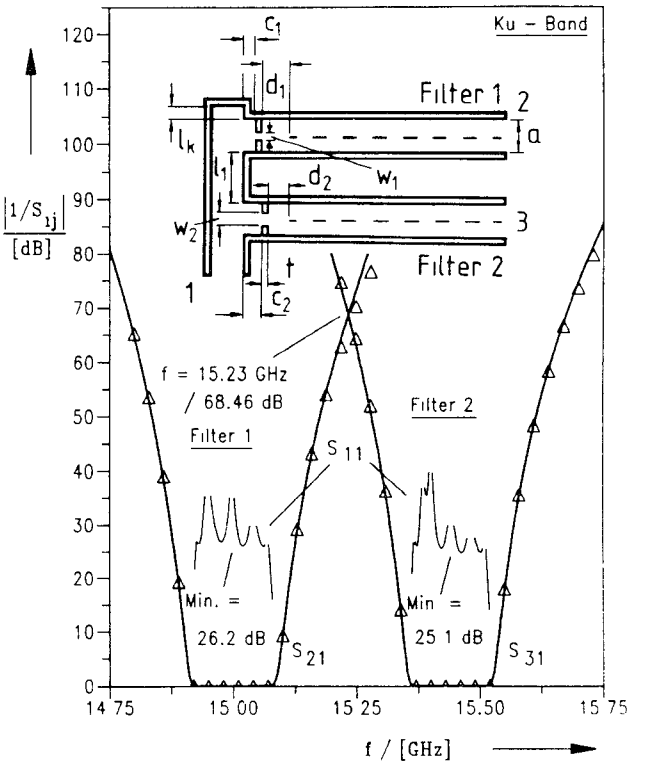

Fig. 5. Computer-optimized *Ku*-band manifold type diplexer with two seven-resonator *E*-plane metal-insert filters. Common port scattering coefficients S_{21} and S_{31} compared with the corresponding single transmission coefficients of the individual filters (Δ Δ Δ). The filter dimensions are given in Table I.

$a = 15.799$ mm, $b = 7.899$ mm, $t = 1$ mm
filter 1: $f_0 = 15$GHz, $B/f_0 = 0.012$
filter 2: $f_0 = 15.44$ GHz, $B/f_0 = 0.0117$
$l_1 = 15.672$ mm, $w_1 = 11.911$ mm, $c_1 = 5.399$ mm, $d_1 = 22.671$ mm
$l_k = 0.052$ mm, $w_2 = 12.2$ mm, $c_2 = 2.871$ mm, $d_2 = 0.052$ mm
(f_0 = midband frequency; B/f_0 = relative bandwidth).

related first filter section; and 4) the corresponding lengths of all waveguide segments between the junctions and between the irises and the junction discontinuities. Parameters 2) to 4) are optimized in the second optimization step.

An optimization strategy factor H, a weighting factor G, and a standard random variable $r \in (-1, +1)$ influence the alternation of the parameter vector $(\bar{x})$ during the optimization process with the deviation $\sigma = H \cdot G$ [21]. The strategy factor H is modified during the optimization program in order to control the speed of convergence. After one or more successful trials, within every three preceding mutations, H is doubled; for more than three unsuccessful trials, H is halved [21]. The weighting factor G may be utilized to modify the variation of the individual parameters $(\bar{x})$. The resonator length variation of the filters should be less than the variation of the coupling sections if, for instance, the ripple behavior has to be improved while the midband frequency behavior of the filter is already satisfactory. The new parameters $(\bar{x})_{\text{new}}$ are calculated at each iteration step by

$$(\bar{x})_{\text{new}} = (\bar{x})_{\text{old}} - r \cdot (\bar{x})_{\text{old}} \cdot \sigma \qquad (5)$$

where $(\bar{x})_{\text{old}}$ are the preceding parameters. Initial values for H and G are chosen to be $H = 0.01$ and $G = 1$. If the error function is minimized three times by less than 0.2 percent, the result is interpreted as a local minimum. H is then multiplied by a large factor (between 10 and 100), which is suitably chosen to guarantee a new start of the optimization outside the local minimum. So the optimization process begins again for a different, perhaps better, parameter range. Note that in order to maintain physically realistic parameters, an appropriate variable transformation [21] is utilized.

Fig. 4 shows the results of a computer-optimized *Ku*-band (12 GHz–18 GHz) common-junction-type diplexer design example with two seven-resonator metallic *E*-plane filters in the main arms of the waveguide (R140 waveguide housing: 15.799 mm ×7.899 mm). The filter dimensions are given in Tables I and II. For a verification of the theory, the common port transmission coefficients, S_{21} and S_{31} of the diplexer (solid lines), are compared with the corresponding single transmission coefficients (Δ Δ Δ) of the individual filters. Good agreement may be stated. The minimum common port return loss in the passbands of the diplexer is 23 dB. Higher return losses may be obtained by a subsequent optimization of the filters. However, in order

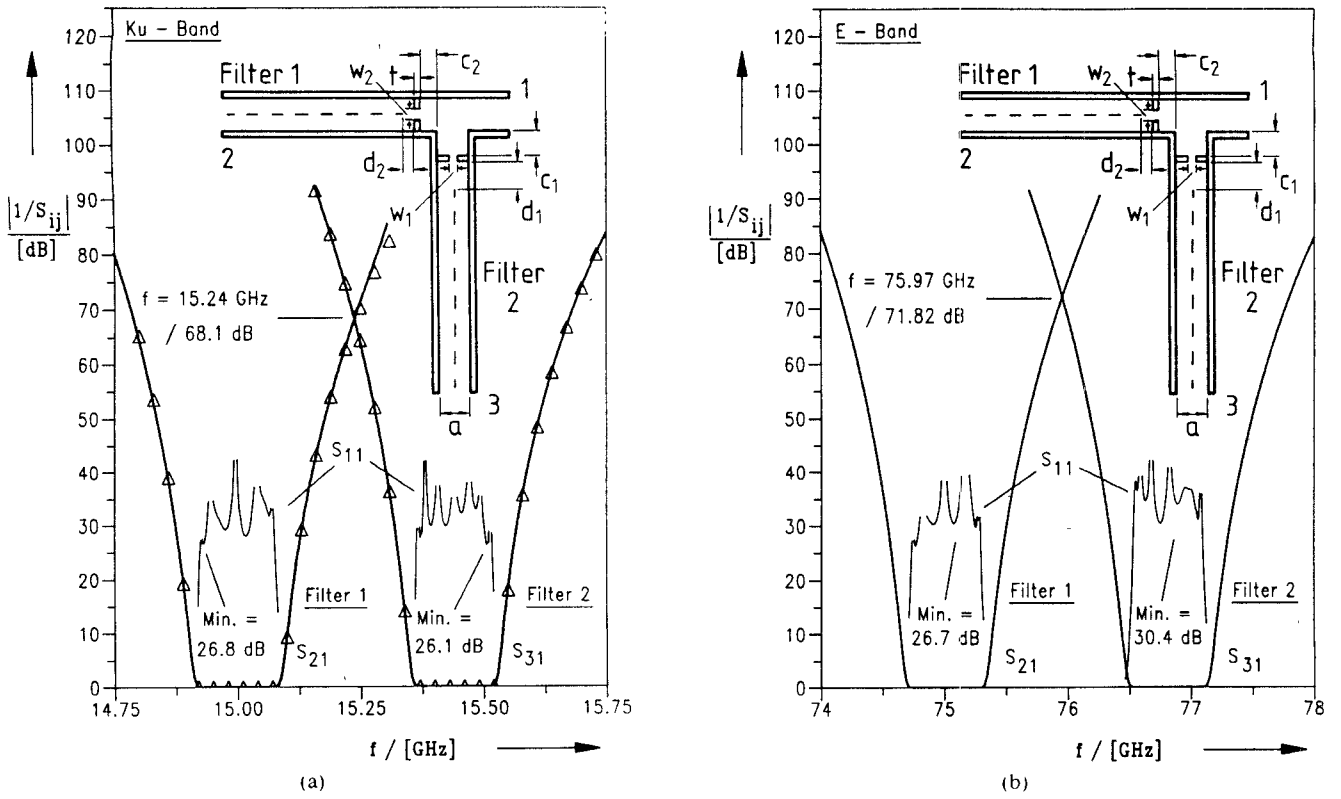

Fig. 6. Computer-optimized modified common junction type diplexer with two seven-resonator E-plane metal-insert filters. Common port scattering coefficients S_{21} and S_{31} compared with the corresponding single transmission coefficients of the individual filters ($\Delta\ \Delta\ \Delta$). The filter dimensions are given in Tables I and II, respectively. (a) Ku-band design example: $a = 15.799$ mm, $b = 7.899$ mm, $t = 1$ mm. Filter 1: $f_0 = 15$ GHz, $B/f_0 = 0.012$. Filter 2: $f = 15.44$ GHz, $B/f_0 = 0.0117$, $w_1 = 9.839$ mm, $c_1 = 3.625$ mm, $d_1 = 9.5$ mm, $w_2 = 12.934$ mm, $c_2 = 3.686$ mm, $d_2 = 5.236$ mm. (b) E-band design example: $a = 3.099$ mm, $b = 1.549$ mm, $t = 0.2$ mm. Filter 1: $f_0 = 75$ GHz, $B/f_0 = 0.00893$. Filter 2: $f_0 = 76.8$ GHz, $/Bf_0 = 0.00872$, $w_1 = 1.959$ mm, $c_1 = 0.781$ mm, $d_1 = 1.970$ mm, $w_2 = 2.442$ mm, $c_2 = 0.790$ mm, $d_2 = 1.022$ mm (f_0 = midband frequency; B/f_0 = relative bandwidth).

to compare the different diplexer configurations with each other, identical filter structures for the three different types of diplexer examples in Figs. 4, 5, and 6(a) have been utilized (cf. Table I).

The computer-optimized Ku-band manifold-type diplexer design example (Fig. 5) yields a common port minimum return loss of 25.1 dB, by using the same filters as in Fig. 4. The best internal compensation potential has been observed in the modified common-junction-type diplexer (Fig 6), which achieves in its Ku-band design version (Fig. 6(a)) a minimum common port return loss of 26.1 dB, and in its E-band (60–90 GHz) version (Fig. 6(b)) 26.8dB. Moreover, the not very distinct first (or last) minimum of the return loss obtained, which is otherwise typically about 30 dB (Fig. 6(a) and (b)) by using the same filters as those of Figs. 4 and 5, indicates that a subsequent filter optimization may yield a further improvement of the minimum return loss value. Again, the transmission coefficients, S_{21} and S_{31} (solid line), demonstrate good coincidence with those of the individual filters ($\Delta\ \Delta\ \Delta$) in Figs. 5 and 6(a).

The theory is verified by comparison of the calculated with the measured common port transmission coefficients

TABLE I
COMPUTER-OPTIMIZED DIMENSIONS (IN MM) OF THE METALLIC E-PLANE FILTERS FOR THE KU-BAND DIPLEXER EXAMPLES

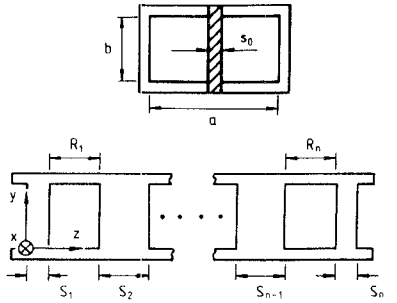

Ku - Band	Filter 3 5 resonators	Filter 4 5 resonators	Filter 1 7 resonators	Filter 2 7 resonators
Fig	7	7	4,5,6a	4,5,6a
S_0	0.190	0.190	0.190	0.190
$S_1 = S_n$	3 111	3.696	3.507	3.970
$S_2 = S_{n-1}$	9 979	11.519	10 971	11.987
$S_3 = S_{n-2}$	11 446	13.215	12.669	13.719
$S_4 = S_{n-3}$			13 034	14 082
$R_1 = R_n$	8 955	7 742	8 961	8.298
$R_2 = R_{n-1}$	8 968	7 717	8 971	8 293
$R_3 = R_{n-2}$	8.968	7 715	8.971	8.293
R_4			8 971	8.293

TABLE II
COMPUTER-OPTIMIZED DIMENSIONS (IN MM) OF THE METALLIC E-PLANE FILTERS FOR THE E-BAND DIPLEXER EXAMPLE

E - Band	Filter 1 7 resonators	Filter 2 7 resonators
Fig.	6b	6b
S_0	0.040	0.040
$S_1 = S_n$	0.731	0.780
$S_2 = S_{n-1}$	2.260	2.371
$S_3 = S_{n-2}$	2.601	2.729
$S_4 = S_{n-3}$	2.674	2.810
$R_1 = R_n$	1.854	1.741
$R_2 = R_{n-1}$	1.857	1.743
$R_3 = R_{n-2}$	1.857	1.743
R_4	1.857	1.743

of a computer-optimized *Ku*-band manifold-type diplexer with five-resonator filters (Fig. 7(a)). The measured minimum return loss was about 17 dB in the first, and 20 dB in the second passband. Although the typical fabrication tolerances of the filter and matching structures, for this example, are within ± 0.02 to ± 0.1 mm, relatively good agreement between measurements and theory may be stated. The diplexer (Fig. 7(b)) has been realized by using a computer-controlled milling machine for the waveguide housings; the metal inserts of the filters have been fabricated by metal-etching techniques. The material of the 190-μm- thick sheet metal is 99.9 percent pure copper.

IV. CONCLUSIONS

The modal S-matrix method described achieves a rigorous computer-aided design of a class of rectangular waveguide slit-coupled H-plane T-junction diplexers utilizing E-plane metal-insert filters. This type of filter permits low-cost manufacturing by accurate and inexpensive metal-etching techniques. The optimization process takes all relevant influences of the complete diplexer structure rigorously into account, such as the finite thickness of the metal inserts and irises and the H-plane T-junction effect. Moreover, the inclusion of the higher order mode interactions at all discontinuities involved yields the advantage of utilizing the full mutual compensation potential inherent in the structure, and allows the stopband characteristics to be included in the diplexer design. Design examples for *Ku*-band (12–18 GHz) and E-band (60–90 GHz) demonstrate the usefulness of the design method. The theory is experimentally verified by a realized diplexer component at *Ku*-band.

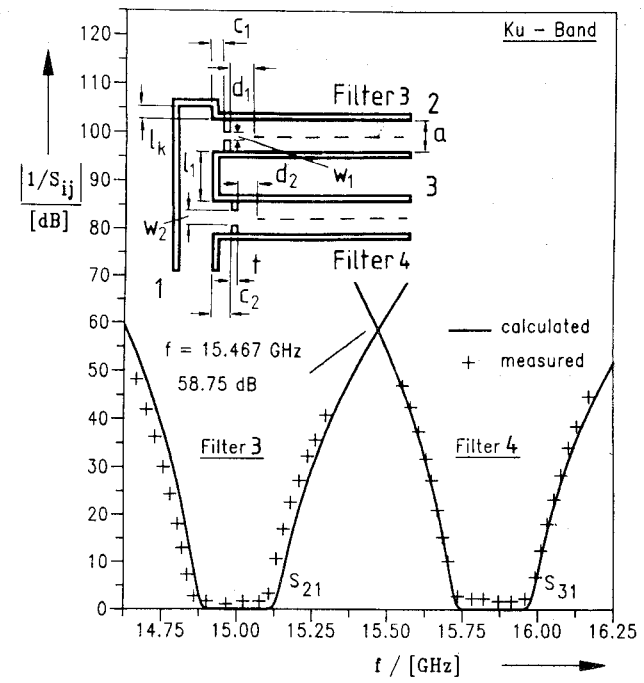

(a)

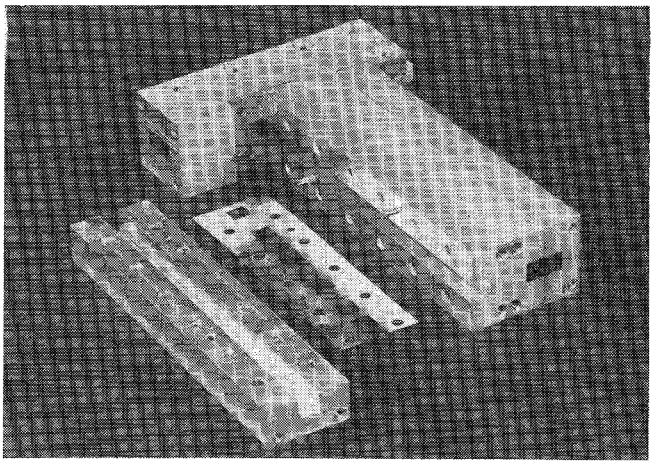

(b)

Fig. 7. Computer-optimized and realized *Ku*-band manifold type diplexer with two five-resonator E-plane metal-insert filters. (a) Calculated common port transmission coefficients S_{21} and S_{31} compared with the measured results (+ + +) (filter dimensions in. Table I):
$a = 15.799$ mm, $b = a/2$, $t = 1$mm
filter 3: $f_0 = 15$ GHz, $B/f_0 = 0.017$
filter 4: $f_0 = 15.85$ GHz, $B/f_0 = 0.016$
$l_1 = 15.920$, $w_1 = 11.012$, $c_1 = 5.745$, $d_1 = 20.018$
$l_k = 0.039$, $w_2 = 12.202$, $c_2 = 2.517$, $d_2 = 0.049$
(all dimensions in mm).
(b) Photograph of the realized component.

APPENDIX

A. Submatrices in Equation (3)

$$(S_{11}) = \underline{V}\left[\underline{T} - \underline{E} - \underline{U}(\underline{E} + \underline{T})^{-1}\underline{U}\right] \quad \text{(A1)}$$

$$(S_{12}) = \underline{V}\underline{U}\left[\underline{E} - (\underline{E} + \underline{T})^{-1}(\underline{T} - \underline{E})\right] \quad \text{(A2)}$$

with the abbreviations

$$\underline{V} = \left[\underline{E} + \underline{T} - \underline{U}(\underline{E} + \underline{T})^{-1}\underline{U}\right]^{-1}, \qquad \underline{E} = \text{unit matrix} \quad \text{(A3)}$$

$$\underline{T} = \sum_{k=1}^{M} \underline{G}^{Lk}\left(\underline{Y}^k + \underline{W}^k\underline{Y}^k\underline{W}^k\right)\left(\underline{G}^{Lk}\right)^t \quad \text{(A4)}$$

where t denotes the transposed matrix, and L denotes the subregion L in Fig. 2(a) and (b) left from $z = 0$.

For the case of the metal strip section of finite length (Fig. 2(a)), the subregions in the middle section to be considered are included by choosing $M = \mathrm{II}$. For the case of the inductive iris section (Fig. 2(b)), M has to be chosen to be $M = \mathrm{I}$.

$$\underline{U} = \sum_{k=\mathrm{I}}^{M} \underline{G}^{Lk}\left(\underline{Y}^{k}\underline{W}^{k} + \underline{W}^{k}\underline{Y}^{k}\right)\left(\underline{G}^{Lk}\right)^{t} \tag{A5}$$

with

$$\underline{Y}^{k} = \left(\underline{E} - \underline{W}^{k}\underline{W}^{k}\right)^{-1} \tag{A6}$$

where $\underline{W}$ is the diagonal matrix of the homogeneous waveguide sections of finite length l with the elements containing the phase terms

$$W_{t}^{k} = e^{-jk_{zhi}^{k}\cdot l}. \tag{A7}$$

The matrices

$$\underline{G}^{Lk} = \underline{D}^{YL}\underline{K}_{hh}^{Lk}\underline{D}^{Zk} \qquad (k = \mathrm{I}, \mathrm{II}) \tag{A8}$$

contain the diagonal matrices with the wave impedances Z,

$$D_{ii}^{YL} = \sqrt{\frac{1}{Z_{hi}^{L}}} = \sqrt{\frac{k_{zhi}}{\omega\mu}} \qquad D_{ii}^{Zk} = \sqrt{Z_{hi}^{k}} \tag{A9}$$

and the matrices with the coupling integrals

$$K_{hh_{ij}}^{Lk} = \left[\omega^{2}\mu\epsilon - \left(k_{zhj}^{k}\right)^{2}\right]\int_{F_k} T_{hi}^{L}\cdot T_{hj}^{k}\cdot df \tag{A10}$$

where k_z is the wavenumber of the TE_{m0} modes in the subregions [20], T_h is the corresponding eigenfunctions of the TE_{m0} modes in the subregions [15], [18]–[20], and F_k is the area of the common interface of the subregion k at the corresponding step discontinuity.

B. Submatrices in Equation (4)

$$(S_{11})_h = (\underline{M}_1\underline{N}_1 + \underline{M}_2) \quad (S_{12})_h = (\underline{M}_1\underline{N}_2 + \underline{M}_3)$$
$$(S_{13})_h = (\underline{M}_1\underline{N}_3 + \underline{M}_1) \tag{A11}$$
$$(S_{21})_h = (\underline{M}_4\underline{N}_1 + \underline{M}_3) \quad (S_{22})_h = (\underline{M}_4\underline{N}_2 + \underline{M}_2)$$
$$(S_{23})_h = (\underline{M}_4\underline{N}_3 + \underline{M}_1) \tag{A12}$$
$$(S_{31})_h = \underline{N}_1, \qquad (S_{31})_h = \underline{N}_2,$$
$$(S_{33})_h = \underline{N}_3 \tag{A13}$$

with the abbreviations

$$\underline{M}_1 = -\underline{D}_1\underline{K}^{\mathrm{II,III}}\underline{D}^{Y,\mathrm{III}} + \underline{D}_2\underline{K}^{\mathrm{I,III}}\underline{D}^{Y,\mathrm{III}} \tag{A14}$$

$$\underline{M}_2 = \underline{D}_1\underline{D}^{Y,\mathrm{I}} - \underline{D}_2\underline{D}^{Y,\mathrm{I}}\underline{D}^{e\mathrm{I}^{-1}} \tag{A15}$$

$$\underline{M}_3 = -\underline{D}_1\underline{D}^{Y,\mathrm{I}}\underline{D}^{e\mathrm{I}^{-1}} + \underline{D}_2\underline{D}^{Y,\mathrm{I}} \tag{A16}$$

$$\underline{M}_4 = \underline{D}_1\underline{K}^{\mathrm{I,III}}\underline{D}^{Y,\mathrm{III}} - \underline{D}_2\underline{K}^{\mathrm{II,III}}\underline{D}^{Y,\mathrm{III}} \tag{A17}$$

$$\underline{N}_1 = \underline{Y}\left(-\underline{K}^{\mathrm{III,I}}\underline{D}^{Y,\mathrm{I}}\underline{M}_2 - \underline{K}^{\mathrm{III,II}}\underline{D}^{Y,\mathrm{I}}\underline{M}_3 - \underline{K}^{\mathrm{III,I}}\underline{D}^{Y,\mathrm{I}}\right) \tag{A18}$$

$$\underline{N}_2 = \underline{Y}\left(-\underline{K}^{\mathrm{III,I}}\underline{D}^{Y,\mathrm{I}}\underline{M}_3 - \underline{K}^{\mathrm{III,II}}\underline{D}^{Y,\mathrm{I}}\underline{M}_2 - \underline{K}^{\mathrm{III,II}}\underline{D}^{Y,\mathrm{I}}\right) \tag{A19}$$

$$\underline{N}_3 = \underline{Y}\left(-\underline{K}^{\mathrm{III,I}}\underline{D}^{Y,\mathrm{I}}\underline{M}_1 - \underline{K}^{\mathrm{III,II}}\underline{D}^{Y,\mathrm{I}}\underline{M}_4 + \underline{D}^{Y,\mathrm{III}}\underline{D}^{e\mathrm{III}-1}\right) \tag{A20}$$

$$\underline{Y} = \left(\underline{K}^{\mathrm{III,I}}\underline{D}^{Y,\mathrm{I}}\underline{M}_1 + \underline{K}^{\mathrm{III,II}}\underline{D}^{Y,\mathrm{I}}\underline{M}_4 - \underline{D}^{Y,\mathrm{III}}\underline{D}^{e\mathrm{III}}\right)^{-1} \tag{A21}$$

$$K_{ln}^{\mathrm{I,III}} = \frac{\frac{n\pi}{2z_1}\frac{l\pi}{2x_1}}{\sqrt{z_1 x_1}}\frac{\sin\left(k_{zhl}^{\mathrm{I}}2z_1\right)}{k_{zhn}^{\mathrm{III}}\left(\frac{1\pi}{2x_1}\right)^{2} - k_{zhn}^{\mathrm{III}2}} \tag{A22}$$

$$k_{pn}^{\mathrm{II,III}} = (-1)^{n}K_{ln}^{\mathrm{I,III}} \tag{A23}$$

$$K_{nl}^{\mathrm{III,I}} = \frac{\frac{l\pi}{2x_1}\frac{n\pi}{2z_1}}{\sqrt{z_1 x_1}}\frac{\sin\left(k_{zhn}^{\mathrm{III}}2x_1\right)}{k_{zhl}^{\mathrm{I}}\left(\frac{n\pi}{2z_1}\right)^{2} - k_{zhl}^{\mathrm{I}^2}} \tag{A24}$$

$$K_{np}^{\mathrm{III,II}} = -(-1)^{n}K_{nl}^{\mathrm{III,I}}. \tag{A25}$$

The elements of the diagonal matrices $\underline{D}^{Y,\mathrm{I}}$, $\underline{D}^{Y,\mathrm{III}}$, $\underline{D}^{e\mathrm{I}}$, and $\underline{D}^{e\mathrm{III}}$ are given by

$$\underline{D}^{e\mathrm{I}} = \begin{pmatrix} \ddots & & \\ & e^{jk_{zm}^{\mathrm{I}}2z_1} & \\ & & \ddots \end{pmatrix}$$

$$\underline{D}^{e\mathrm{III}} = \begin{pmatrix} \ddots & & \\ & e^{jk_{xm}^{\mathrm{III}}2x_1} & \\ & & \ddots \end{pmatrix} \tag{A26}$$

$$D_{i}^{Y,\mathrm{I}} = \sqrt{\frac{1}{Z_{h_i}^{\mathrm{I}}}}$$

$$D_{i}^{Y,\mathrm{III}} = \sqrt{\frac{1}{Z_{h_i}^{\mathrm{III}}}}. \tag{A27}$$

Diagonal matrices $\underline{D}_1$ and $\underline{D}_2$ are given by

$$\underline{D}_1 = \underline{D}^{e\mathrm{I}^{-1}}\underline{D}_2 \tag{A28}$$

$$\underline{D}_2 = \left(\underline{D}^{Y,\mathrm{I}}\underline{D}^{e\mathrm{I}}\right)^{-1}\left(\underline{E} - \underline{D}^{e\mathrm{I}^{-1}}\underline{D}^{e\mathrm{I}^{-1}}\right)^{-1}. \tag{A29}$$

References

[1] G. L. Matthaei, L. Young, and E. M. T. Jones, "*Microwave Filters, Impedance-Matching Networks, and Coupling Structures.*" New York: McGraw-Hill, 1964, ch. 13, 16.

[2] J. L. Haine and J. D. Rhodes, "Direct design formulas for asymmetric bandpass channel diplexers," *IEEE Trans. Microwave Theory Tech.*, vol MTT-25, pp. 807–814, Oct. 1977.

[3] J. D. Rhodes and R. Levy, "A generalized multiplexer theory," *IEEE Trans Microwave Theory Tech.*, vol. MTT-27, pp. 99–111, Feb. 1979.

[4] J. D. Rhodes and R. Levy, "Design of general manifold multiplexers," *IEEE Trans. Microwave Theory Tech.*, vol. MTT-27, pp. 111–123, Feb. 1979.

[5] J. Reindel, "Printed WG circuits trim component costs," *Microwaves*, pp. 60–63, Oct. 1980.

[6] K. D. Breuer and N. Worontzoff, "Low cost multiplexer for channelized receiver front ends at millimeter waves," in *IEEE MTT-S Int. Symp. Dig.* 1980, pp. 150–152.
[7] P. J. Meier *et al.* "Channelized receiver covering 26 to 60 GHz with planar integrated-circuit elements," in *IEEE MTT-S Int. Symp. Dig.* 1981, pp. 411–413.
[8] L. D. Cohen, N. Worontzoff, J. Levy, and A. Harvey, "Millimeter wave multiplexer with printed circuit elements for the 88 to 100 GHz frequency range," in *IEEE MTT-S Int. Symp. Dig.*, 1984, pp. 233–235.
[9] F. Arndt, J. Bornemann, D. Grauerholz, D. Fasold, and N. Schroeder, "Waveguide *E*-plane integrated-circuit diplexer," *Electron. Lett.* vol. 21, pp. 615–617, July 4, 1985.
[10] C. Nguyen and K. Chang, "*W*-band wideband low loss planar integrated circuit diplexer," *Microwave J.*, pp. 157–161, July 1985.
[11] Y.-C. Shih and T. Itoh, "Millimeter-wave diplexers with printed circuit elements," *IEEE Trans. Microwave Theory Tech.*, vol. MTT-33, pp. 1465–1469, Dec. 1985.
[12] Y.-C. Shih, L. Q Bui, and T. Itoh, "Mm-wave contiguous diplexer designed with printed circuit elements," *Microwave Syst. News*, vol. 17, pp. 46–53, Feb. 1987.
[13] D. Rubin and A. R. Hislop, "Millimeter-wave coupled line filters," *Microwave J.*, pp. 67–78, Oct. 1980.
[14] Y. Konishi and K. Uenakada, "The design of a bandpass filter with inductive strip—Planar circuit mounted in waveguide," *IEEE Trans. Microwave Theory Tech.*, vol. MTT-22, pp. 869–873, Oct. 1974.
[15] R. Vahldieck, J. Bornemann, F. Arndt, and D. Grauerholz, "Optimized waveguide *E*-plane metal insert filters for millimeter-wave applications," *IEEE Trans. Microwave Theory Tech.*, vol. MTT-31, pp. 65–69, Jan. 1983.
[16] Y.-C. Shih and T. Itoh, "*E*-plane filters with finite-thickness septa," *IEEE Trans. Microwave Theory Tech.*, vol. MTT-31, pp. 1009–1013, Dec. 1983.
[17] J. W. Bandler, S. Daijavad, and Q.-J. Zhang, "Exact simulation and sensitivity analysis of multiplexing networks," *IEEE Trans. Microwave Theory Tech.*, vol. MTT-34, pp. 93–101, Jan. 1986.
[18] F. Arndt *et al.*, "Modal *S*-matrix method for the optimum design of inductively direct-coupled cavity filters," *Proc. Inst. Elec. Eng.*, vol. 133, pt. H, pp. 341–350, Oct. 1986.
[19] H. Schmiedel and F. Arndt, "Numerical synthesis of simple waveguide mode sensors," in *13th European Microwave Conf. Proc.*, Sept. 1983, pp. 145–150,
[20] R. E. Collin, *Field Theory of Guided Waves*. New York: McGraw-Hill, 1960, ch. 1, 5, 6, 8.
[21] H. Schmiedel, "Anwendung der Evolutionsoptimierung bei Mikrowellenschaltungen," *Frequenz*, vol. 35, pp. 306–310, Nov. 1981.
[22] F. Arndt, I. Ahrens, U. Papzinier. U. Wiechmann, and R. Wilkeit, "Optimized *E*-plane T-junction series power dividers," *IEEE Trans. Microwave Theory Tech.*, vol. MTT-35, pp. 1052–1059, Nov. 1987.
[23] J. Dittloff, J. Bornemann, and F. Arndt, "Computer aided design of optimum *E*- or *H*-plane *n*-furcated waveguide power dividers," in *Proc. Europ. Microwave Conf.* (Rome), Sept. 1987, pp. 181–186,
[24] J. Bornemann and F. Arndt, "Modal-*S*-matrix design of optimum stepped ridged and finned waveguide transformers," *IEEE Trans. Microwave Theory Tech.*, vol. MTT-35, pp. 561–567, June 1987.
[25] H. Schmiedel, "Feldtheoretische Analyse und Synthese von Modenkopplern," *Frequenz*, vol. 37, pp. 207–214, Aug. 1983.

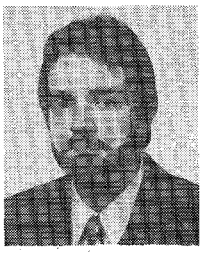

Joachim Dittloff was born on January 6, 1959, in Rotenburg (Wümme), West Germany. He received the Dipl.-Ing., and Dr.-Ing. degrees from the University of Bremen, West Germany, in 1984 and 1987, respectively, for research in microwave applications.

Since 1984 he has been with the Microwave Department of the University of Bremen. His work is on rectangular waveguide components (phase shifters, power dividers, multiplexing structures, and filters).

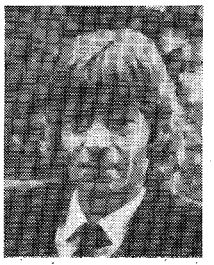

Fritz Arndt (SM'83) received the Dipl. Ing., Dr. Ing., and Habilitation degrees from the Technical University of Darmstadt, Germany, in 1963, 1968, and 1972, respectively.

From 1963 to 1973, he worked on directional couplers and microstrip techniques at the Technical University of Darmstadt. Since 1972, he has been a Professor and Head of the Microwave Department of the University of Bremen, Germany. His research activities are in the area of the solution of field problems of waveguide, finline, and optical waveguide structures, of antenna design, and of scattering structures.

Dr. Arndt is member of the VDE and NTG (Germany). He received the NTG award in 1970, the A. F. Bulgin Award (together with three coauthors) from the Institution of Radio and Electronic Engineers in 1983, and the best paper award of the Antenna Conference JINA 1986 (France).